Applied Catalysis B: Environmental 129 (2013) 146–152

Contents lists available at SciVerse ScienceDirect

Applied Catalysis B: Environmental

journal homepage: www.elsevier.com/locate/apcatb

Surface reconstruction enhancing activity of Pt/C for formic acid electrooxidation by ultrasonic mixing with Pb/C and electrochemical activation process

Xiao Zhao[a,b], Jianbing Zhu[a,b], Liang Liang[c], Chenyang Li[c], Changpeng Liu[c,*], Wei Xing[a,*]

[a] State Key Laboratory of Electroanalytical Chemistry, Changchun Institute of Applied Chemistry, Chinese Academy of Sciences, Jilin, 5625 Renmin Street, Changchun 130022, China
[b] Graduate School of the Chinese Academy of Sciences, Beijing 100039, China
[c] Laboratory of Advanced Power Sources, Changchun Institute of Applied Chemistry, 5625 Renmin Street, Changchun 130022, China

ARTICLE INFO

Article history:
Received 14 June 2012
Received in revised form 15 August 2012
Accepted 28 August 2012
Available online 4 September 2012

Keywords:
Surface reconstruction
Formic acid fuel cell
Platinum
Lead
Ultrasonic mixing
Electronic effect
Third-body effect

ABSTRACT

The control for surface of catalysts is intrinsically required to improve catalytic efficiency. In current work, we demonstrate that the surface of Pt/C catalyst can be effectively reconstructed by ultrasonic mixing with Pb/C in an acidic environment and electorchemical activation process. As a result, the surface-reconstructed Pt/C catalyst exhibits a significant enhancement of activity of a ca. 10-fold improvement in mass activity and a ca. 38-fold improvement in specific activity as compared with a pure Pt/C catalyst for formic acid electroxidation (FAEO). The evidences show that some of Pb species are transferred from Pb/C to surface of Pt/C catalyst probably through the dissolution–adsorption pathway during ultrasonic mixing and electorchemical activation processes. The presence of Pb on surface of Pt not only isolates the continuous Pt sites through the third-body effect but also modifies electronic band structure of platinum via electronic effect, which leads to that the direct pathway is preferably occurred and the CO formation is effectively inhibited. These results provide useful information for further understanding the promotion mechanism of Pb ad-atom during FAEO and rationally controlling the catalytic surface to improve catalytic efficiency.

1. Introduction

Driven by the demand of clean and high-efficiency energy conversion devices, direct formic acid fuel cells (DFAFCs) have received considerable attentions due to the fuel of formmic acid possessing fast oxidation kinetics, less toxicity, lower crossover rate [1–3]. One key challenge for developing DFAFCs is the fabrication of efficient and durable catalysts for formic acid electrooxidation (FAEO) [4–13]. Platinum is one of the most efficient metal catalyst for fuel cell reaction [14–19], however, it is easily poisoned by the CO-like intermediate produced from the incomplete oxidation of fuel.

Modification of Pt with foreign metal (Me = Pb, Bi, Au and Sb etc.) is known to enhance the rate of FAEO [6,11,20–25]. Although no agreement on the origin of this enhancement is achieved up to now, it is generally ascribed to any or all of the following: the third-body of effect, electronic interaction and bifunctional mechanism [1,26,27]. PtPb-based catalyst is one of the most active catalyst and has received the increasing attention for FAEO. For example, a significantly enhanced activity has been observed on intermetallic Pt-Pb nanoparticles (NPs) [23,28]. The modified Pt by under-potential deposition of Pb aslo obtained the enhaced activity for FAEO [24,29]. Although advances have been achieved, there is a demand for a simple and effective preparation of active PtPb-based catalyst. On the other hand, the control for surface of catalyst is of significant interest to improve catalytic efficiency of catalyst. Early studies showed that the controlling coverage degree of Bi, Pb adatoms on Pt electrode through the potential step or under-potential deposition method can lead to the significantly enhanced activity of Pt electrode for FAEO[30,31,32]. Recent advance have been focused on the controlled surface for the nano-sized particles with the purpose of the better utilizaiton of noble metal such as the submonolayer Pt-decorated Au NPs [20]. However, the preparation of these catalyst involves the multi-setp procedure and the sophisticatd experiment technique which limit their large-scale application to some exent.

In this work, using a simple strategy, we demonstrate that the surface of Pt/C catalyst can be effectively reconstructed by ultrasonic mixing with Pb/C in an acidic environment and electorchemical activation process. As a result, the surface-reconstructed Pt/C catalyst (denoted as Pt/C + Pb/C catalyst) exhibits a significant enhancement of activity of a ca. 10-fold improvement in mass activity and a ca. 38-fold improvement in specific activity as compared with a pure Pt/C catalyst for FAEO. The physical and electrochemical characterizaitons show evidences that some of Pb species are

* Corresponding authors. Tel.: +86 431 85262223; fax: +86 431 85685653.
E-mail addresses: liuchp@ciac.jl.cn (C. Liu), xingwei@ciac.jl.cn (W. Xing).

0926-3373/$ – see front matter © 2012 Elsevier B.V. All rights reserved.
http://dx.doi.org/10.1016/j.apcatb.2012.08.028

transferred from Pb/C to surface of Pt in Pt/C + Pb/C catalyst probably through the dissolution–adsorption pathway during ultrasonic mixing and electorchemical activation processes.

2. Experimental

2.1. Catalyst preparation

2.1.1. The synthesis of Pb/C and Au/C

The 20 wt% Pb/C was prepared by a chemical reduction method. Specifically 80 mg of Vulcan XC 72 carbon, 32 mg lead nitrate and 42 mg sodium citrate were ultrasonically dispersed in 100 mL of deionised water to form a uniform suspension. Under stirring, a fresh $NaBH_4$ solution (50 mL, 0.36 mg mL^{-1}) was added drop by drop to reduce Pb precursor. Finally, the suspension was filtered, and the obtained Pb/C was washed with warm deionised water and dried in a vacuum oven at 60 °C overnight. The 20 wt% Au/C was prepared using a similar procedure with the synthesis of Pb/C, except that the 2 mL $HAuCl_4$ solution (10 mg_{Au} mL^{-1}) replaced the 32 mg lead nitrate. The 20 wt% Pt/C catalyst was purchased from Johnsom Matthey Company (HiSPEC^{TM} 3000).

2.1.2. The synthesis of Pt/C + Pb/C and Pt/C + Au/C catalysts

The Pt/C + Pb/C catalyst was prepared by the ultrasonic mixing of Pt/C with Pb/C. Specifically, the as-prepared 2.6 mg Pb/C and the commercial 2.4 mg Pt/C were added into the solution of 0.95 mL ethanol and 0.05 mL Nafion ionomer. The resulting mixture was ultrasonically mixed to form a uniform catalyst ink for the following physical and electrochemical characterizations. The Pt/C + Au/C was prepared using a similar procedure with the synthesis of Pt/C + Pb/C except that 2.5 mg Au/C and 2.5 mg Pt/C replaced 2.6 mg Pb/C and 2.4 mg Pt/C, respectively.

2.1.3. The preparation of Pb/C, Au/C and Pt/C catalyst inks

The catalyst inks for Pb/C, Au/C and Pt/C were prepared using a similar procedure with the synthesis of Pt/C + Pb/C except that 5 mg Pb/C, 5 mg Au/C and 5 mg Pt/C replaced the mixture of 2.6 mg Pb/C and 2.4 mg Pt/C, respectively. For consistency, these catalyst inks were also directly used for the following physical and electrochemical characterizations.

2.2. Catalyst characterization

The size and morphology of catalyst were analyzed by transmission electron microscopy (TEM) and high-resolution (HR) TEM operating at 200 kV (Philips TECNAI G2). The sample for TEM characterization was prepared by diluting the catalyst ink by a factor of 100 in anhydrous ethanol and subsequently placing a drop of prepared solution on a carbon-coated copper grid and drying at room temperature. The X-ray diffraction (XRD) patterns of the catalysts were obtained using a PW1700 diffractometer (Philips Co.) with a Cu Kα (λ = 0.15405 nm) radiation source operating at 40 kV and 30 Ma. X-ray photoelectron spectroscopy (XPS) measurement was conducted using an ESCALAB MKII photoelectron spectrometer (VG Scientific). The sample for XRD and XPS characterization was obtained by directly dropping catalyst ink on a glass substrate to form a thick catalyst film.

2.3. Electrochemical measurements

All electrochemical measurements were carried out with an EG&G mode 273 potentiostat/galvanostat and a conventional three-electrode test cell at the ambient temperature. 5 μL of the as-prepared catalyst ink was pipetted and spread on the 3 mm-diameter pre-cleaned glassy carbon disk as the working electrode. A Pt foil and a saturated calomel electrode (SCE) were used as the counter and reference electrodes, respectively. To evaluate the activity of catalysts for FAEO, the cyclic voltammetry (CV) and linear scan voltammetry (LSV) experiments were carried out in 0.5 M H_2SO_4 + 0.5 M HCOOH solution with a scan rate of 50 mV s^{-1}. The chronoamperometric experiments were performed in the same solution at the potential of 0.2 V vs. SCE for 3600 s. The electrochemical surface areas (ESA) of catalysts were estimated by under-potential hydrogen assuming that the coulombic charge required for the oxidation of the hydrogen monolayer is 210 μC cm^{-2}. All electrolyte solutions were deaerated by high-purity nitrogen for at least 10 min prior to any measurements. To avoid the Pb contaminant, all electrolyte solutions were afresh prepared after the every measurement of Pb/C and Pt/C + Pb/C.

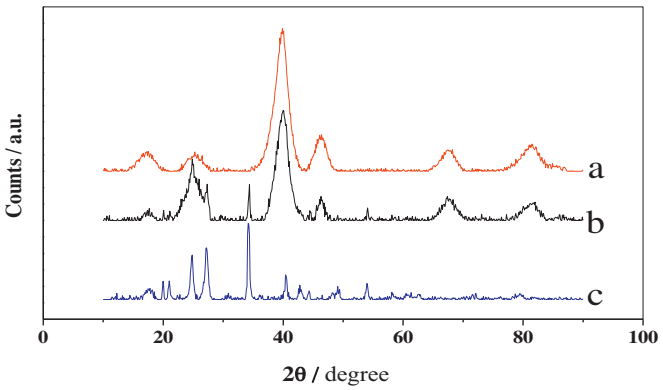

Fig. 1. XRD patterns of Pt/C (a), Pt/C + Pb/C (b) and Pb/C (c) catalysts.

3. Results and discussion

Fig. 1 presents the XRD patterns of Pb/C, Pt/C + Pb/C and Pt/C catalysts. From Fig. 1a, Pt/C exhibits the typical character of a crystalline Pt face-centered cubic phase. The Pb/C shows a set of character peaks at 24.83, 27.32, 34.27 and 54.08 assigned to diffraction peaks of $PbCO_3$-$Pb(OH)_2$ indicating the Pb NPs is oxidized at ambient environment which is consistent with the previous report [33,34]. The crystalline structure of Pt/C + Pb/C catalyst shows the coexistence of Pt peaks and Pb peaks demonstrating that ultrasonic mixing process has no appreciable effect on the respective crystalline structure of Pt/C and Pb/C component. The broad diffraction feature at 2θ = 12–22° can be assigned to the diffraction of the polyfluorocarbon chains of Nafion [35].

In order to investigate morphology and dispersion of Pt NPs, the TEM analysis was conducted. Fig. 2 manifests the representative TEM images of Pt/C and Pt/C + Pb/C catalysts. Most of Pt NPs for both Pt/C and Pt/C + Pb/C catalysts are uniformly dispersed on the surface of carbon support with a narrow size distribution. The specific size distributions are obtained by measuring the sizes of 100 randomly selected particles in the magnified TEM images. The average particle size of Pt/C catalysts is approximately 2.96 nm. The Pt/C + Pb/C catalyst displays a average size of 3.12 nm which is slightly greater than the size of Pt/C. Note that Pt/C + Pb/C catalyst was prepared using Pt/C and Pb/C precursors in which Pt and Pb NPs have been anchored on the surface of carbon support before the treatment of ultrasonic mixing. The ultrasonic mixing alone should have few influences on the dispersion and the size variation for the anchored Pt NPs. Thus, Pt/C and Pt/C + Pb/C catalysts display near particle size and size distribution. In order to reveal the microstructure of Pt/C and Pt/C + Pb/C catalysts, HRTEM was applied to characterize respective Pt NPs. As shown in Fig. 2g and h, the both of d-spacing between the Pt {1 1 1} planes are ca. 0.225 nm for Pt/C and Pt/C + Pb/C catalysts, which is well accordance with the results of XRD. For Pt/C + Pb/C catalyst as shown

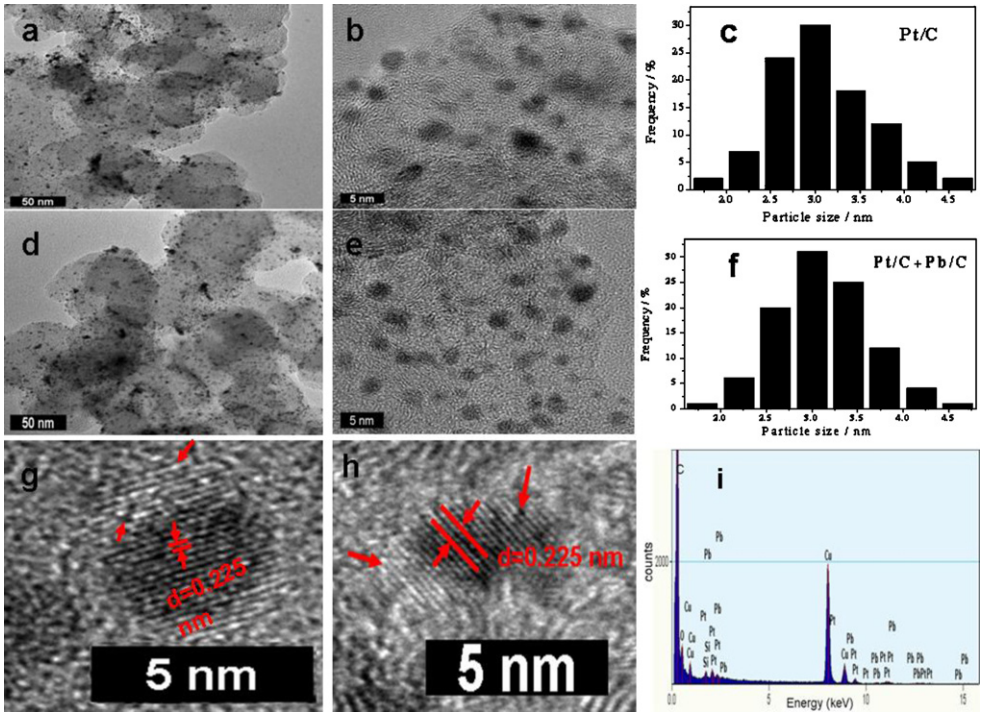

Fig. 2. TEM images and corresponding size distributions of Pt/C (a–c), Pt/C + Pb/C (d–f); HRTEM images of Pt/C + Pb/C (g), Pt/C (h) catalysts; EDX spectra of Pt/C + Pb/C catalyst (i).

in Fig. 2g, we can observe the contrast difference between the edge and center of the particle and the overlaping darkness dot signed by arrows which seem to indicate the presence of Pb species on Pt surface induced by the ultrasonic mixing process. While, in Fig. 2h of Pt/C catalyst, similar situation signed by arrows was also found athough less obvious than that of Pt/C + Pb/C catalyst. In combination of these TEM observations and themslevs small difference in imaging contrast between Pt and Pb, it is not yet sufficient to estimate the presence of Pb species on Pt surface of Pt/C + Pb/C catalyst in current stage. Fig. 2i shows the EDX spectrum of Pt/C + Pb/C catalyst. The co-existence of Pt and Pb characteristic peaks reveals that Pt/C and Pb/C were successfully mixed together.

Although TEM is reliable to directly oberve the microstructure of Pt NPs, it only detect a limited number of NPs. In contrast, the electrochemical methods can provide overall structural information of catalysts. Fig. 3a compares the activity of Pb/C, Pt/C + Pb/C and Pt/C electrodes for FAEO by LSV measurements in 0.5 M H_2SO_4 + 0.5 M HCOOH at a scan rate of 50 mV s^{-1}. Before applied for FAEO, Pb/C, Pt/C + Pb/C and Pt/C electrodes were electrochemically activated in 0.5 M H_2SO_4 solution by voltammetric method from −0.242 to 0.958 vs. SCE until the reproducible CV curves were obtained. It is generally accepted that FAEO on Pt electrode follows a dual-pathway mechanism: the direct pathway involves a fast reaction via a reactive intermediate and the indirect pathway includes the formation of poisoning CO species. The stable LSV profile of Pt/C electrode is characterized by two anodic peaks (at ca. 0.243 V and ca. 0.673 V vs. SCE). The first oxidation peak at ca. 0.243 V can be assigned to the direct oxidation of formic acid into CO_2; while the second anodic peak at 0.673 V corresponds to the oxidation of CO species adsorbed Pt surface. Thus, the ratio of I_{P1} to I_{P2} was usually used to reflect the tolerance of catalyst to CO poisoning [36,37]. The I_{P1}/I_{P2} for Pt/C + Pb/C electrode is ca. 2.7 which is much higher than that for Pt/C catalyst (0.58) indicating better tolerance to CO poisoning and enhanced activity. What is more, the mass activity at 0.2 V for Pt/C + Pb/C electrode is 1280 mA mg_{Pt}^{-1} exhibiting ca. 10 times improvement compared with Pt/C catalyst (118 mA mg_{Pt}^{-1}). The Pb/C shows no appreciable activity for FAEO. In addition, the onset potential of FAEO for Pt/C + Pb/C electrode is cathodically shifted by 130 mV as compared with Pt/C electrode. To compare the intrinsic activities of catalysts, the current density was normalized with ESA. From the inset in Fig. 3a, Pt/C + Pb/C electrode displays a ca. 38-fold improvement in intrinsic activity compared with Pt/C electrode. Fig. 3b illustrates the current–time curves of electrodes recorded at 0.2 V vs. SCE. According to the inset in Fig. 3b, the stable current density on Pt/C + Pb/C electrode is 4.2 times larger than that

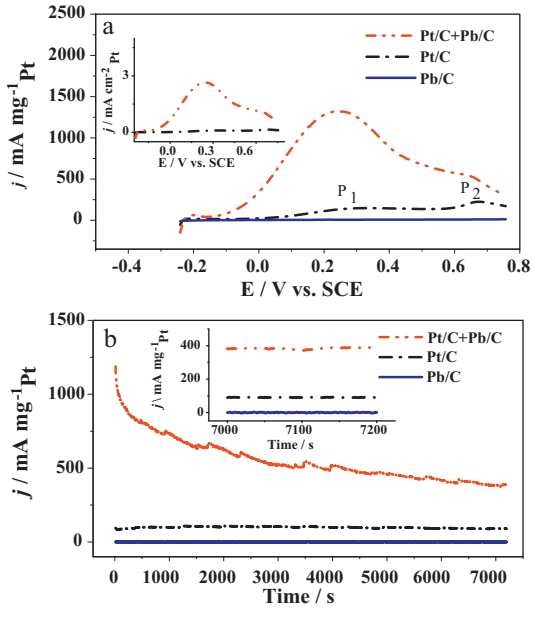

Fig. 3. The mass activity of catalysts evaluated by LSV measurements in 0.5 M HCOOH+0.5 M H_2SO_4 at a scan rate of 50 mV s^{-1}, the inset shows the corresponding specific activity of catalysts (a). Current–time curves of catalysts recorded at 0.2 V vs. SCE in the same solution, the inset shows the magnified curves (b).

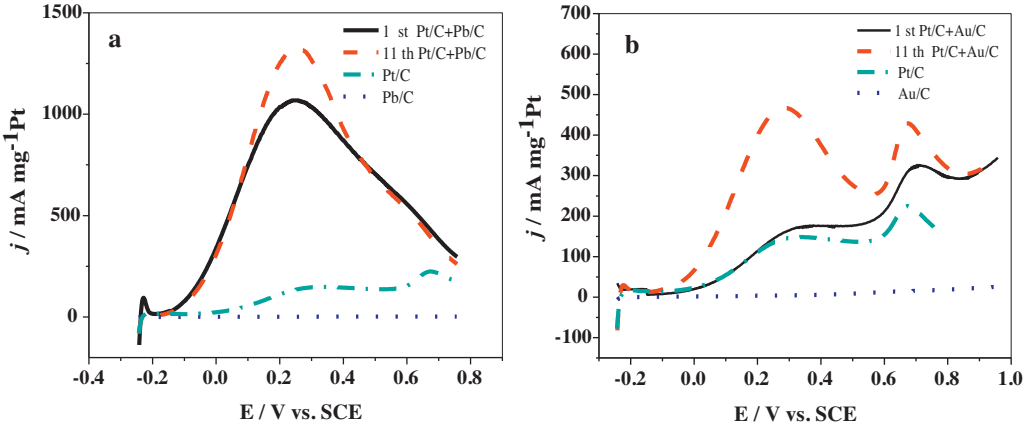

Fig. 4. To understand the influence of ultrasonic mixing alone on the catalytic behavior of Pt/C + Pb/C electrode, the freshly prepared (i.e. electrochemically un-activated) Pt/C + Pb/C electrode was directly used to catalyze FAEO. For clarity, only positive-scan cyclic voltammograms were shown for Pt/C + Pb/C electrode (a) and Pt/C + Au/C electrode (b) in 0.5 M HCOOH + 0.5 M H_2SO_4 at a scan rate of 50 mV s^{-1}. The freshly prepared Pt/C + Au/C electrode was used as a reference for comparison.

on Pt/C electrode. The deactivation rate for the Pt/C + Pb/C electrode is ca 3.8%/100 s in the first 1000 s. This is better than that of 3 nm palladium NPs with a deactivation rate of 4.5%/100 s [2]. It is noteworthy that Pt/C electrode shows well stability, but exhibits very low activity due to CO poisoning. From the above results, it is safe to conclude that Pt/C + Pb/C electrode clearly exhibits a superior activity for FAEO compared with Pt/C electrode.

To understand the influence of ultrasonic mixing alone on the catalytic behavior of Pt/C + Pb/C electrode, the freshly prepared (i.e. electrochemically un-activated) Pt/C + Pb/C electrode was directly used to catalyze FAEO. Fig. 4a displays the positive-scan CV curves of the freshly prepared Pt/C + Pb/C electrode in 0.5 M H_2SO_4 + 0.5 M HCOOH solution at a scan rate of 50 mV s^{-1}. It is clearly that the first CV curves for Pt/C + Pb/C electrode exhibit a significantly enhanced catalytic activity for FAEO relative to Pt/C electrode, particularly in the low potential region. The I_{P1}/I_{P2} for the first cycle of Pt/C + Pb/C electrode is ca. 2.5 which is much higher than that for Pt/C electrode (0.58). Because the kinetics of FAEO is highly sensitive to the surface of electrode [38,39], the enhanced activity strongly indicates that the surface of Pt in the freshly-prepared Pt/C + Pb/C electrode has been largely reconstructed just during ultrasonic mixing process. After 11 potential cycles, Pt/C + Pb/C electrode shows slightly higher peak current than that of the first CV curve indicative of electrochemical potential cycles also generating an influence on the activity of Pt/C + Pb/C electrode. These results reveal that the surface of Pt/C + Pb/C electrode can be reconstructed and modified in both ultrasonic mixing and electrochemical potential cycle processes.

In order to further understand the effect of ultrasonic mixing and electrochemical activation processes on the reconstruction of catalytic surface, the control experiment was conducted by using Pt/C + Au/C electrode as a reference. The profile of the first CV curves for Pt/C + Au/C electrode shows the similar profile of CV curves with Pt/C electrode revealing that the Pt surface of Pt/C + Au/C electrode is almost unchanged in the ultrasonic mixing process. This can be attributed to that the noble metal of Au is hard to oxidize and dissolve and therefore the surface reconstruction for Pt/C + Au/C electrode is difficult to occur in the current ultrasonic mixing process. However, after 11 potential cycles, the profile of CV curves for Pt/C + Au/C electrode shows a clearly enhanced activity compared with the profile of first CVs curves particularly in the low potential zone. According to the comparison between Pt/C + Pb/C and Pt/C + Au/C electrodes, it seems plausible that during ultrasonic mixing process, the Pb as base metal in relation to Au is easily oxidized, dissolved and adsorbed on Pt surface in the presence of Nafion ionomer, which in turn significantly affects the activity of Pt/C + Pb/C electrode. In other words, during the current ultrasonic mixing process the surface-reconstruction for Pt/C + Pb/C catalyst is much easily occurred compared with Pt/C + Au/C electrode and probably through the dissolution–adsorption pathway. However, when the proper potential window was chosen to activate the electrodes, voltammetric activation process facilitates the surface-reconstruction and generates the influence on activity for both Pt/C + Au/C and Pt/C + Pb/C electrodes.

The hydrogen adsorption/desorption is well-known structure-sensitive reaction and can be used to confirm the corresponding change in Pt surface of Pt/C + Pb/C electrode. Fig. 5 displays the stable CV curves for Pt/C and Pt/C + Pb/C electrodes in 0.5 M H_2SO_4 solution at a scan rate of 50 mV s^{-1}. The hydrogen adsorption/desorption peaks and the Pt oxidation/reduction peaks are clearly observed for both Pt/C + Pb/C and Pt/C electrodes. However, the area of hydrogen desorption peak for Pt/C + Pb/C electrode is much smaller than that of Pt/C electrode verifying a reduced ESA for Pt/C + Pb/C electrode. Specifically, the ESA for Pt/C + Pb/C electrode calculated from under-potential hydrogen is reduced by ca. 71.5% compared with the ESA of Pt/C electrode. What is more, the shape of hydrogen adsorption/desorption for Pt/C + Pb/C electrode becomes featureless instead of the well-defined characteristic peaks as observed in the CV curves of Pt/C electrode. In combination with the above control experiment, the reduced ESA for Pt/C + Pb/C electrode is most probably due to that Pb species cover the Pt active sites.

The surface-reconstructed Pt NPs for Pt/C + Pb/C catalyst can be further confirmed by the observation of XPS. Fig. 6a displays the

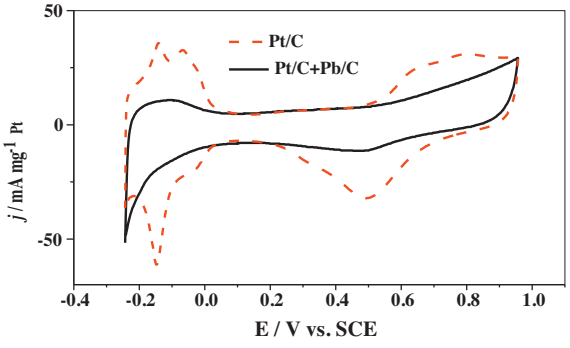

Fig. 5. Cyclic voltammograms of Pt/C and Pt/C + Pb/C electrodes recorded in a N_2-purged 0.5 M H_2SO_4 solution at a scan rate of 50 mV s^{-1}.

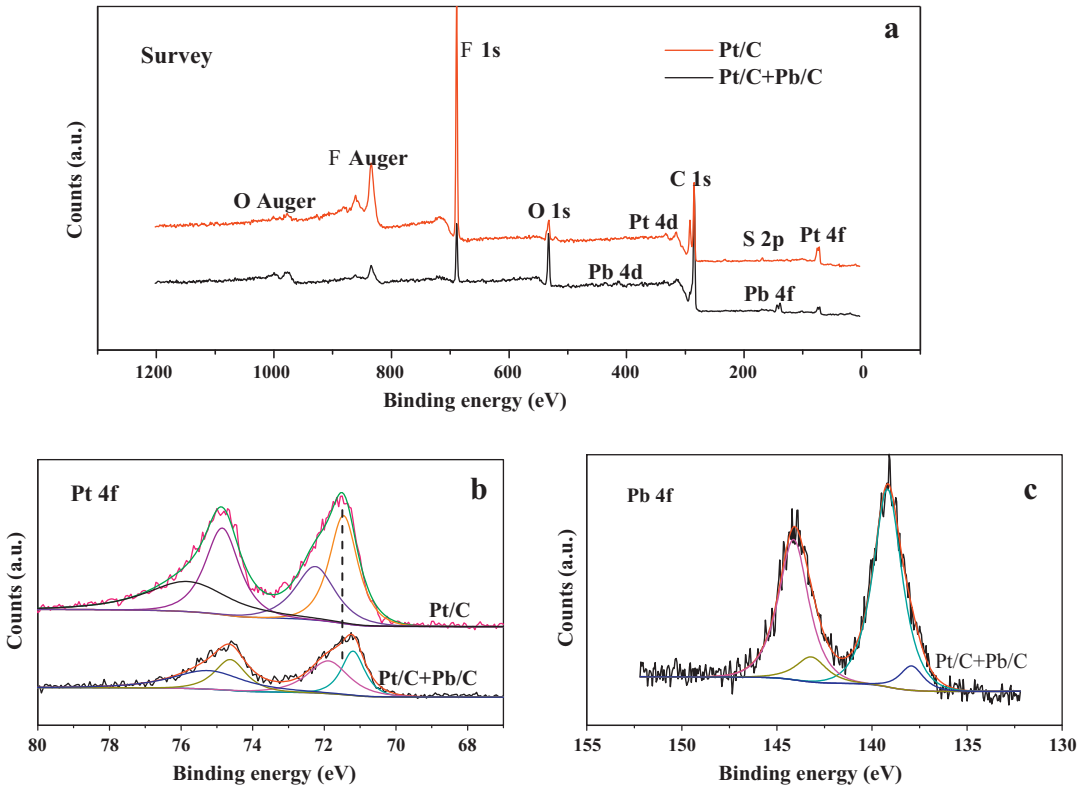

Fig. 6. XPS spectra of Pt/C and Pt/C + Pb/C catalysts: survey spectra (a), the comparison of Pt 4f region for Pt/C and Pt/C + Pb/C catalysts (b) and Pb 4f region of Pt/C + Pb/C catalyst (c).

survey spectra of Pt/C + Pb/C and Pt/C catalysts. As expected, the spectrum of Pt/C + Pb/C catalyst shows Pb characteristics peaks. The F and S element in spectra of Pt/C + Pb/C and Pt/C catalysts can be assigned to the Nafion ionomer. Fig. 6b exhibits the comparison of Pt 4f region of two catalysts. There are two distinct peaks assigned to the Pt $4f_{7/2}$ and Pt $4f_{5/2}$ regions which can be deconvolved into metallic Pt and Pt (II) species. By comparison, the binding energies (BE) of Pt 4f for Pt/C + Pb/C catalyst are shifted to low BE direction compared with Pt/C catalyst. Specifically, the BE of Pt $4f_{7/2}$ for Pt/C catalyst are 71.4 eV and 72.2 eV, assigned to metallic Pt and Pt (II) species respectively, while those for Pt/C + Pb/C catalyst are 71.2 eV and 71.9 eV, respectively. This negative shift in BE of Pt 4f indicates the changed Pt surface for Pt/C + Pb/C catalyst and is most likely due to the Pb modifying the Pt electronic structure. Generally, the shift of Pt 4f position indicates an electronic effect which can influence the catalytic properties [1,15,40]. Fig. 6c shows the Pb 4f spectrum of Pt/C + Pb/C catalyst. By deconvolution, Pb 4f signal of Pt/C + Pb/C catalyst displays the characteristics of Pb (II) species at 139.2 and 144.1 eV, and Pb (IV) species at 137.9 and 143.2 eV. The XPS analysis evidently shows that lead is easily oxidized to lead oxide at ambient environment, which is in accordance with the XRD pattern of Pb/C and the previous reports [27,34].

From the above characterizations, the reasons for the enhanced activity of Pt/C + Pb/C catalyst can be rationalized as follows. First, evidences showed that the direct pathway of FAEO on Pt electrode needs only individual Pt atoms but the indirect pathway needs an ensemble of Pt atoms [36]. In this respect, the "third-body effect" works well by isolating the continuous Pt atoms [21,36,41,42]. Specifically, the addition of a second element (third body) to Pt reduces the number of ensemble sites for the production of CO_{ads} due to geometrical hindrance and therefore the poisoned Pt sites by CO_{ads} are much less than the pure Pt surface. For Pt/C + Pb/C catalyst, the reduced ESA and the negative shift in BE of Pt 4f both strongly indicate the presence of Pb on Pt surface which leads to the isolated Pt sites due to the geometric hindrance of Pb. The much-enhanced activity at low potential and the higher value of I_{P1}/I_{P2} for Pt/C + Pb/C catalyst also verify the isolated Pt sites on which the direct pathway is preferably occurred and CO formation is effectively inhibited. Thus, the "third-body effect" should be responsible for the dramatically enhanced activity. Second, XPS analysis shows the direct evidence on the modified Pt electronic structure for Pt/C + Pb/C catalyst which may activate the Pt metal and contribute to the enhancement of catalytic activity. This can be justified by the negative-shift in onset potential of FAEO and the enhanced intrinsic activity for Pt/C + Pb/C catalyst. Thus the electronic effect is considered to be an important factor which leads to the activation of Pt NPs and thus accelerates the kinetic rate of FAEO on Pt/C + Pb/C catalyst.

Furthermore, we show the concern on durability of Pt/C + Pb/C catalyst in the accelerated durability tests (ADT) although Pt/C + Pb/C catalyst has showed the significantly enhanced activity and respectful stability. The ADT was carried out by potential cycling between −0.242 and 0.758 V vs. SCE in 0.5 M H_2SO_4 + 0.5 M HCOOH solution at a scan rate of 50 mV s^{-1}. Fig. 7a shows the change of activity of Pt/C + Pb/C electrode. After 200 potential cycles, peak current density of Pt/C + Pb/C electrode has reduced by approximately 36.5% as compared with the first CV curves of Pt/C + Pb/C electrode. Meanwhile, the shape of P_2 became prominent, which resembles FAEO behaviors of monometallic Pt and indicates that partial Pt surface has been recovered due to that Pb tends to leach out under current ADT conditions. Generally, the degradation of Pt-based catalyst can be caused by the loss of ESA due to active particle dissolution and growth and carbon corrosion, as well as the decrease in intrinsic activity caused by change in their surface composition. For example, Ru dissolution and crossover was found to cause the degradation of PtRu catalyst in a long-term operation of methanol fuel cell [15,43]. However, it should be noted that in some designed activating processes, the

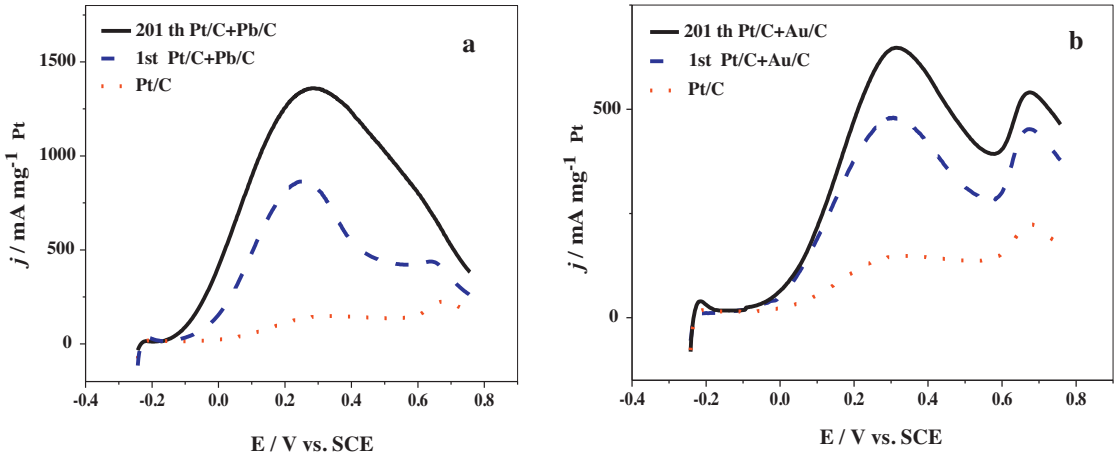

Fig. 7. The accelerated durability tests of activated Pt/C + Pb/C electrode (a) and activated Pt/C + Au/C electrode (b) carried out by potential cycling between −0.242 and 0.758 V vs. SCE in 0.5 M H_2SO_4 + 0.5 M HCOOH solution at a scan rate of 50 mV s^{-1}. For clarity, only positive-scan cyclic voltammograms were shown.

change in surface composition may lead to the increase in intrinsic activity. Typically, Strasser et al. [44,45] demonstrated that by voltammetric dissolution of Cu from surface layer of PtCu alloy, the as-obtained dealloyed PtCu catalyst exhibited an extraordinary increase in intrinsic reactivity of 4–6 times as compared to pure Pt catalyst for oxygen reduction reaction. In this case, the voltammetric dissolution of Cu was believed to lead to the catalytic surface reconstruction from the Pt–Cu bimetallic alloy surface to the Pt-rich compressive surface and thereby results in a shift of the electronic band structure of Pt and a weakening chemisorption of oxygenated species. An activation of potential cycling or anodic oxidation was also usually adopted to activate the PtRu catalyst and generate beneficial RuO_xH_y species [46,47]. Similarly, the currently investigated Pt/C + Pb/C catalyst showed evidences that some of Pb species were transferred from Pb/C to Pt surface of Pt/C + Pb/C catalyst probably through the dissolution–adsorption route in the activating stage, which results in the Pb modified Pt surface and thus the enhanced activity for FAEO. However, when extending the time-scale of test and applying a rigorous test condition such as the current ATD, this kind of irreversible oxidation-dissolution process ultimately deteriorates the activity of catalyst as observed in PtRu catalyst [15,43,48] and current Pt/C + Pb/C catalyst. For the degradation of Pt/C + Pb/C catalyst in ADT, the Pt particle dissolution-growth and the Pb oxidation-dissolution interrelated occurred and both of them should be responsible for the degradation of Pt/C + Pb/C catalyst.

The durability of Pt/C + Au/C electrode was also evaluated by ADT. To avoid the Pb contaminant, all electrolyte solutions were afresh prepared. The result for Pt/C + Au/C electrode is shown in Fig. 7b. Interestingly, the peak current density of Pt/C + Au/C electrode after 200 potential cycling shows a clear improvement for FAEO compared with the first CVs curves. This increased activity strongly indicates the presence of other promoting effect against the degradation of catalyst caused by the loss of ESA. It was recently reported that modifying Pt NPs with Au clusters could effectively stabilize the Pt catalyst against dissolution by raising the Pt oxidation potential [49]. Meanwhile, it was verified that either Au on Pt NPs or Pt on Au NPs both possessed the dramatically improved activity for FAEO compared with pure Pt catalyst [20,21,30]. These factors may generate a contrary effect on the decline in activity of Pt/C + Au/C electrode although dissolution-growth of NPs still occurred during ADT. Comprising these contradictory effects, Pt/C + Au/C electrode, therefore, enables a net improvement of activity in current ADT. In addition, Au itself possesses much higher resistance to electrochemical corrosion compared with the base metal of Pb. Combining these considerations, PtAu catalyst such as PtAu alloy [50] and Pt on Au nanocatalyst [20] should represent a class of active and durable catalyst for FAEO compared with Pt/C catalyst. However, it is important to note that due to Pt and Au being both noble metals, the PtAu catalyst may bring out the challenge of catalyst cost if considering their large-scale application in DFAFC. Thus combining the catalyst cost and current experiment results, PtAuPb trimetallic catalyst may be a class of promising catalyst with high activity and durability for FAEO such as the nanostructured PtPb@PtAu core–shell catalyst.

4. Conclusions

In summary, the surface of Pt/C catalyst was effectively reconstructed by ultrasonic mixing with Pb/C in an acidic electrolyte and electorchemical activation process. Electrochemical studies and physical analyses indicate that some of Pb species were transferred from Pb/C to Pt surface of Pt/C + Pb/C catalyst during activation processes. The third-body effect and electronic effect are responsible for the improved activity of Pt/C + Pb/C catalyst for FAEO. The current structure-activity analysis would be helpful for further understanding the promoting effect of Pb. However, Pt/C + Pb/C catalyst shows inferior durability compared to Pt/C + Au/C catalyst in the long-term life tests. Taking catalyst cost and catalytic performance into account, the nanostructured PtPb@PtAu core–shell catalyst may be promising catalyst used in the anode of formic acid fuel cell. Some attempts are underway in our group.

Acknowledgments

This work was supported by the National Natural Science Foundation of China (nos. 20703043, 21073180, 21011130027 and 20933004), the National High Technology Research and Development Program of China (863 Program, no. 2012AA053401), the National Basic Research Program of China (973 Program, 2011CB935702, 2012CB215500 and 2012CB932800), the Knowledge Innovation Project of CAS (KGCXZ-Y10-344) and the Science & Technology Research Programs of Jilin Province (nos. 20102204, 20100420).

References

[1] X.W. Yu, P.G. Pickup, Journal of Power Sources 182 (2008) 124–132.
[2] J. Ge, W. Xing, X. Xue, C. Liu, T. Lu, J. Liao, Journal of Physical Chemistry C 111 (2007) 17305–17310.

[3] M. Ren, Y. Kang, W. He, Z. Zou, X. Xue, D.L. Akins, H. Yang, S. Feng, Applied Catalysis B: Environmental 104 (2011) 49–53.
[4] B. Fang, M. Kim, J.-S. Yu, Applied Catalysis B: Environmental 84 (2008) 100–105.
[5] S. Murugesan, K. Myers, V. Subramanian, Applied Catalysis B: Environmental 103 (2011) 266–274.
[6] V. Selvaraj, M. Alagar, K.S. Kumar, Applied Catalysis B: Environmental 75 (2007) 129–138.
[7] D. Tu, B. Wu, B. Wang, C. Deng, Y. Gao, Applied Catalysis B: Environmental 103 (2011) 163–168.
[8] G. Zhang, Y. Wang, X. Wang, Y. Chen, Y. Zhou, Y. Tang, L. Lu, J. Bao, T. Lu, Applied Catalysis B: Environmental 102 (2011) 614–619.
[9] X. Zhao, Y. Hu, L. Liang, C. Liu, J. Liao, W. Xing, International Journal of Hydrogen Energy 37 (2012) 51–58.
[10] X. Zhao, J. Zhu, L. Liang, C. Liu, J. Liao, W. Xing, Journal of Power Sources 210 (2012) 392–396.
[11] S. Zhang, Y. Shao, G. Yin, Y. Lin, Angewandte Chemie International Edition 49 (2010) 2211–2214.
[12] G. Zhang, Y. Wang, X. Wang, Y. Chen, Y. Zhou, Y. Tang, L. Lu, J. Bao, T. Lu, Applied Catalysis B 102 (2011) 614–619.
[13] Tu. Dandan, B. Wu, B. Wang, C. Deng, Y. Gao, Applied Catalysis B 103 (2011) 163–168.
[14] J. Xu, G. Fu, Y. Tang, Y. Zhou, Y. Chen, T. Lu, Journal of Materials Chemistry 22 (2012) 13585–13590.
[15] X. Zhao, M. Yin, L. Ma, L. Liang, C. Liu, J. Liao, T. Lu, W. Xing, Energy & Environmental Science 4 (2011) 2736–2753.
[16] M.K. Debe, Nature 486 (2012) 43–51.
[17] Y. Chen, Y. Zhou, Y. Tang, T. Lu, Journal of Power Sources 195 (2010) 4129–4134.
[18] Y. Chen, G. Zhang, J. Ma, Y. Zhou, Y. Tang, T. Lu, International Journal of Hydrogen Energy 35 (2010) 10109–10117.
[19] X. Zhao, J. Zhu, L. Liang, J. Liao, C. Liu, W. Xing, Journal of Materials Chemistry (2012), http://dx.doi.org/10.1039/C2JM33926A.
[20] N. Kristian, Y.S. Yan, X. Wang, Chemical Communications 44 (2008) 353–355.
[21] R.Y. Wang, C. Wang, W.B. Cai, Y. Ding, Advanced Materials 22 (2010) 1845–1848.
[22] X. Zhou, C.C. Liu, J.P. Liao, T.H. Lu, W. Xing, Journal of Power Sources 179 (2008) 481–488.
[23] E. Casado-Rivera, D.J. Volpe, L. Alden, C. Lind, C. Downie, T. Vazquez-Alvarez, A.C.D. Angelo, F.J. DiSalvo, H.D. Abruna, Journal of the American Chemical Society 126 (2004) 4043–4049.
[24] S. Uhm, H.J. Lee, Y. Kwon, J. Lee, Angewandte Chemie International Edition 47 (2008) 10163–10166.
[25] F.J. Vidal-Iglesias, J. Solla-Gullon, E. Herrero, A. Aldaz, J.M. Feliu, Angewandte Chemie International Edition 49 (2010) 6998–7001.
[26] J.L. Haan, K.M. Stafford, R.I. Masel, Journal of Physical Chemistry C 114 (2010) 11665–11672.
[27] X.W. Yu, P.G. Pickup, Electrochimica Acta 55 (2010) 7354–7361.
[28] L.R. Alden, D.K. Han, F. Matsumoto, H.D. Abruna, F.J. DiSalvo, Chemistry of Materials 18 (2006) 5591–5596.
[29] S.Y. Uhm, S.T. Chung, J.Y. Lee, Electrochemistry Communications 9 (2007) 2027–2031.
[30] S. Motoo, M. Watanabe, Journal of Electroanalytical Chemistry and Interfacial Electrochemistry 98 (1979) 203–211.
[31] M. Shibata, S. Motoo, Journal of Electroanalytical Chemistry and Interfacial Electrochemistry 188 (1985) 111–120.
[32] X.H. Xia, T. Iwasita, Journal of The Electrochemical Society 140 (1993) 2559–2565.
[33] D.J. Chen, Z.Y. Zhou, Q. Wang, D.M. Xiang, N. Tian, S.G. Sun, Chemical Communications 46 (2010) 4252–4254.
[34] D.R. Blasini, D. Rochefort, E. Fachini, L.R. Alden, F.J. DiSalvo, C.R. Cabrera, H.D. Abruna, Surface Science 600 (2006) 2670–2680.
[35] Z.G. Shao, P. Joghee, I.M. Hsing, Journal of Membrane Science 229 (2004) 43–51.
[36] M. Neurock, M. Janik, A. Wieckowski, Faraday Discussions 140 (2008) 363–378.
[37] W. Chen, J.M. Kim, S.H. Sun, S.W. Chen, Langmuir 23 (2007) 11303–11310.
[38] J. Clavilier, R. Parsons, R. Durand, C. Lamy, J.M. Leger, Journal of Electroanalytical Chemistry 124 (1981) 321–326.
[39] J. Solla-Gullon, F.J. Vidal-Iglesias, A. Lopez-Cudero, E. Garnier, J.M. Feliu, A. Aldaza, Physical Chemistry Chemical Physics 10 (2008) 3689–3698.
[40] K.W. Park, J.H. Choi, B.K. Kwon, S.A. Lee, Y.E. Sung, H.Y. Ha, S.A. Hong, H. Kim, A. Wieckowski, Journal of Physical Chemistry B 106 (2002) 1869–1877.
[41] E. Leiva, T. Iwasita, E. Herrero, J.M. Feliu, Langmuir 13 (1997) 6287–6293.
[42] U.B. Demirci, Journal of Power Sources 173 (2007) 11–18.
[43] P. Piela, C. Eickes, E. Brosha, F. Garzon, P. Zelenay, Journal of the Electrochemical Society 151 (2004) A2053–A2059.
[44] P. Strasser, S. Koh, T. Anniyev, J. Greeley, K. More, C.F. Yu, Z.C. Liu, S. Kaya, D. Nordlund, H. Ogasawara, M.F. Toney, A. Nilsson, Nature Chemistry 2 (2010) 454–460.
[45] S. Koh, P. Strasser, Journal of the American Chemical Society 129 (2007) 12624.
[46] Q.Y. Lu, B. Yang, L. Zhuang, J.T. Lu, Journal of Physical Chemistry B 109 (2005) 1715–1722.
[47] L. Ma, C.P. Liu, J.H. Liao, T.H. Lu, W. Xing, J.J. Zhang, Electrochimica Acta 54 (2009) 7274–7279.
[48] A. Taniguchi, T. Akita, K. Yasuda, Y. Miyazaki, Journal of Power Sources 130 (2004) 42–49.
[49] J. Zhang, K. Sasaki, E. Sutter, R.R. Adzic, Science 315 (2007) 220–222.
[50] S. Zhang, Y.Y. Shao, H.G. Liao, J. Liu, I.A. Aksay, G.P. Yin, Y.H. Lin, Chemistry of Materials 23 (2011) 1079–1081.